What is the contribution of convergence zones to global precipitation? Assessing observations and climate models biases

JGR Atmospheres

RESEARCH ARTICLE
10.1029/2023JD039635

What Is the Contribution of Convergence Zones to Global Precipitation? Assessing Observations and Climate Models Biases

Gabriel M. P. Perez[1,2], Pier Luigi Vidale[1,3], Helen Dacre[1], and Thomas C. M. Martin[2]

[1]Department of Meteorology, University of Reading, Reading, UK, [2]MeteoIA, Sao Paulo, Brazil, [3]National Centre for Atmospheric Science, Reading, UK

Key Points:

- Approximately 54% of global precipitation falls over convergence zones
- Climate models overestimate this ratio by approx. 10%
- Conservative moisture advection schemes seem to alleviate this overestimation

Supporting Information:

Supporting Information may be found in the online version of this article.

Correspondence to:

G. M. P. Perez,
gabriel@meteoia.com

Citation:

Perez, G. M. P., Vidale, P. L., Dacre, H., & Martin, T. C. M. (2024). What is the contribution of convergence zones to global precipitation? assessing observations and climate models biases. *Journal of Geophysical Research: Atmospheres*, *129*, e2023JD039635. https://doi.org/10.1029/2023JD039635

Received 12 JULY 2023
Accepted 10 APR 2024

Author Contributions:

Conceptualization: Gabriel M. P. Perez, Pier Luigi Vidale, Helen Dacre
Formal analysis: Gabriel M. P. Perez
Funding acquisition: Pier Luigi Vidale
Investigation: Gabriel M. P. Perez
Methodology: Gabriel M. P. Perez, Pier Luigi Vidale, Helen Dacre, Thomas C. M. Martin
Software: Gabriel M. P. Perez, Thomas C. M. Martin
Supervision: Pier Luigi Vidale, Helen Dacre
Validation: Gabriel M. P. Perez, Thomas C. M. Martin
Writing – original draft: Gabriel M. P. Perez
Writing – review & editing: Gabriel M. P. Perez

Abstract Convergence zones (CZs) are known drivers of precipitation regimes from regional to planetary scales. However, there is a scarcity of accounts of the contribution of CZs to the global precipitation. In this study, we build upon a recently developed Lagrangian diagnostic to attribute precipitation to CZ events in observations and simulations submitted to the Coupled Model Intercomparison Project 6 (CMIP6). Observed CZs are identified using ERA5 reanalysis wind and attributed precipitation from observational products based on satellite estimates and rain gauges. We estimate that approximately 54% (51%–59%, depending on the precipitation product) of global precipitation falls over CZs; in some regions, such as the Intertropical Convergence Zone (ITCZ) and subtropical monsoon regions, this proportion is greater than 60%. All CMIP6 simulations analyzed here attribute about 10% more precipitation to CZ events than what the observations suggest. To investigate this overestimation, we decompose the precipitation error in terms of frequency and intensity of CZ precipitation and find that all models present a substantial positive bias in the frequency of CZ precipitation, suggesting that climate models trigger precipitation too easily in regions of airmass confluence; such positive frequency biases in CZ precipitation help explaining well-known biases in climate models, such as the double-ITCZ in the Pacific. We also find that models with better mass conservation present an apportionment of CZ precipitation closest to the observational estimates, demonstrating the relevance of mass conservation in advection schemes.

Plain Language Summary Rain is crucial for human and animal livelihoods. In the Earth's atmosphere, rain often occurs in organized cloud bands of hundreds or thousands of kilometers lengthwise. This type of organized rain is usually denominated as occurring within a convergence zone (CZ). In this study, we use a recently developed method to identify these CZs and apply it to observational data to find out how much of Earth's rain falls in regions under the influence of CZs (approximately 54%). We repeat this exercise in climate model data and find that all models overestimate rain in regions under the influence of CZs by about 10%. Our results point to the importance of CZs for the global hydrological cycle and ways in which climate models need improvement to better simulate CZ rainfall.

1. Introduction

Advection by the low-level horizontal flow reshapes the atmospheric moisture distribution so as to support large-scale organized precipitation features; this occurs around well-known features associated with the confluence of airmasses (Here we refer to airmass as bodies of air with a similar origin in space) such as fronts, the Intertropical Convergence Zone (ITCZ) and subtropical convergence zones (CZs) (Cohen & Kreitzberg, 1997; Kodama, 1992). Generally, we will be referring to these phenomena as CZs. Most algorithms to identify CZs are region specific, that is, they are calibrated to capture rainfall or cloudiness bands with certain local characteristics (Carvalho et al., 2004; Van Der Wiel et al., 2016). The case of fronts is an exception; fronts can be objectively detected by thermodynamic parameters and precipitation in their neighborhood can be masked (Catto et al., 2015). However, such parameters are not effective in the tropics and subtropics, where airmass boundaries are not expected to show a clear signature in thermodynamic variables.

Eulerian approaches based on low-level wind fields are commonly used to identify CZs. For example, Weller et al. (2017) apply an Eulerian deformation metric on 6-hourly wind fields to identify convergence lines in the low-level flow. The authors further mask precipitation around these lines using a fixed-distance criterion and estimate that between 55% and 96% of the precipitation (between 60°N and 60°S) is associated with these

convergence lines, with large differences in the estimates over land and ocean. A shortcoming of their approach is that the instantaneous convergence field over land is noisy, resulting in climatologies that are hard to interpret. Moreover, Eulerian convergence lines do not necessarily favor moisture accumulation as the pathlines along which moisture is transported diverge from the instantaneous streamlines within the median lifetime of water vapor, which is approximately 4 days (Läderach & Sodemann, 2016).

The ability to associate precipitation with weather phenomena, such as CZs, is an important step in identifying and understanding the causes of model biases and enabling the improvement of models as well as of their use (Leung et al., 2022). Important biases in mean precipitation are still present in Coupled Model Intercomparison Project 6 (CMIP6) simulations (Li et al., 2021), limiting the reliability of future climate simulations. The double-ITCZ is one such problem that has been present in CMIP3, CMIP5 and still persists in CMIP6 (Tian & Dong, 2020); Zhou et al. (2022) link this problem to a drizzling bias in climate models. Catto et al. (2015) have shown that, in the mid-latitude winter, errors in the frequency and intensity of frontal precipitation also explain a substantial portion of the precipitation biases in CMIP5 models.

In this study we define CZ precipitation as precipitation occurring within regions where the Lagrangian kinematics of the synoptic-scale flow favors the accumulation of moisture. We build upon the mixing diagnostic developed in Perez et al. (2021) to propose a spatio-temporal masking technique that allows the allocation of precipitation to CZs. We then adapt the decomposition in Catto et al. (2015) to perform a process-based evaluation of precipitation biases in CMIP6 models in terms of frequency and intensity of CZ precipitation. The scientific questions we aim to answer are the following:

1. What fraction of global precipitation falls within CZs?
2. Are climate models capable of representing this apportionment?
3. What is the contribution of frequency and intensity of CZ precipitation to model biases?

2. Synoptic-Scale Mixing and Precipitation

Filaments of high tracer concentration in the atmosphere arise as a consequence of mixing, which is defined as the stretching and folding of material contours caused by advection (Methven & Hoskins, 1999; Ottino, 1989; Welander, 1955). Mixing can be quantified by the finite-time Lyapunov exponent (FTLE), a measure of the Lagrangian deformation of neighboring parcels (Pierrehumbert, 1991; Shepherd et al., 2000). When trajectories are computed to represent pathways of water vapor, FTLE features identify flow structures that promote moisture accumulation (Perez et al., 2021). Some key considerations have to be made in order to find such relevant moisture pathways: (a) the duration of the back-trajectories to be considered and (b) the flow in which the trajectories are computed. Here we follow the approach in Perez et al. (2021, 2022) and compute 2-day back-trajectories in a horizontal flow derived from a vertical weighting that accounts for moisture concentration at each vertical level; we note that 2 days is well within the median residence time of water vapor (Läderach & Sodemann, 2016). A similar approach was adopted by Garaboa-Paz et al. (2015) and Garaboa-Paz et al. (2017) to investigate atmospheric rivers as FTLE features.

FTLE features computed as described above quantify the purely kinematical effect of mixing in enhancing existing moisture gradients via advection. The intensity of the effect of FTLE features on precipitation will therefore depend on the existing background moisture distribution and on the presence of vertical motion that enables parcel saturation and precipitation, such as slantwise ascent or convection. Indeed, Perez et al. (2022) show that the sensitivity of monthly mean precipitation to the FTLE varies across the globe; particularly, this relationship is stronger in tropical and subtropical regions, where total column water vapor is typically higher than in the extratropics. In the next section, we describe a masking technique to assign precipitation to CZs that accounts for the spatially dependent mixing-precipitation relationship.

3. Convergence Zone Precipitation Mask

We allocate precipitation to CZ events in a given grid-box based on two criteria: (a) the FTLE is positive, meaning that air parcels arriving at the CZ are approximating each other in a 2-day time interval and (b) the FTLE value of that grid-box is higher than a threshold σ'. The threshold σ' is defined per grid-box as a function of the probability of a precipitation event occurring: σ' is the FTLE value of a quantile that is as frequent as a precipitation event $P > 1$ mm/day in that grid-box. It can be written as:

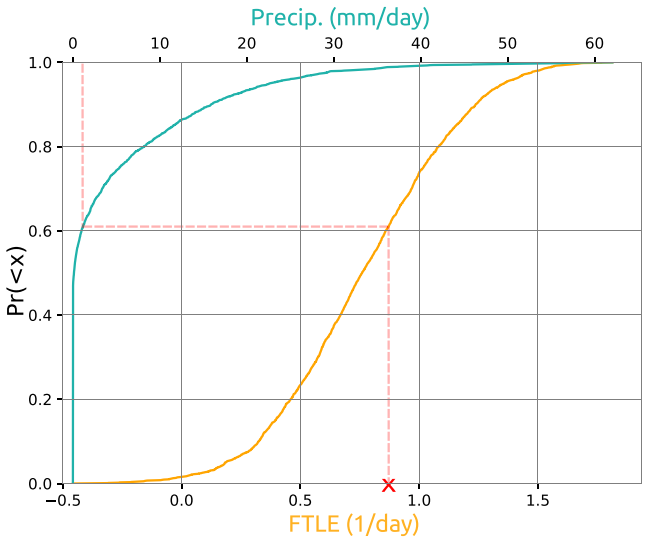

Figure 1. Look-up process to determine the finite-time Lyapunov exponent (FTLE) threshold σ' based on a precipitation event of 1 mm/day. The orange and light green curves represent respectively the cumulative distribution function (CDF) of the FTLE and precipitation at the grid-box closest to São Paulo, Brazil (23.5°S, 46.5°W). The dashed red lines illustrate the transformation of the 1 mm/day precipitation threshold into an FTLE threshold by comparing the two CDFs.

$$\sigma' = F_\sigma \left[F_P^{-1} \left(P > 1 \frac{mm}{day} \right) \right] \quad (1)$$

where F_P^{-1} is the inverse cumulative distribution function (CDF) of precipitation and F_σ is the CDF of the FTLE. This look-up process is illustrated in Figure 1.

Assigning precipitation to CZs when the FTLE exceeds the spatially dependent threshold σ' serves two purposes: (a) it compensates for the meridional variation in mean FTLE values, which are typically higher at higher latitudes and (b) it accounts for the spatially dependent mixing-precipitation relationship described in Section 2. That is, if precipitation events are rare (extreme) in a given region, CZ precipitation is masked with equally extreme FTLE contours. In the same way, if precipitation is very frequent, we will look for FTLE contours that occur frequently.

The threshold of $P > 1$ mm/day is chosen to define precipitation events in order to avoid the drizzle problem in climate models; that is, CMIP6 models precipitate very small amounts too frequently (Chen et al., 2021; Zhou et al., 2022). Catto et al. (2015) finds that employing this threshold brings the ratio of rainy days in models closer to the satellite estimates. Therefore, precipitation amounts below 1 mm/day are set to zero.

Figure 2 illustrates the procedure with the observational data sets on a particular day. Figure 2a shows the FTLE and the contours where the FTLE exceeds σ' (i.e., the CZ mask). Figure 2b shows GPCP-1DD precipitation on the same date and the precipitation contours that overlap with the CZ mask. All precipitation enclosed by the red contours in Figure 2b is assigned to CZs. Similar masking procedures have been used with other process-based diagnostics to assess the contributions of fronts (Catto et al., 2015) and tropical cyclones (Franco-Diaz et al., 2019; Guo et al., 2017) to the hydrological cycle. A key difference between our CZ mask and the one employed in Weller et al. (2017) is the width or shape of our contours is variable because it depends on the FTLE values, whilst Weller et al. (2017) mask precipitation within a fixed 2° distance of the Eulerian convergence lines.

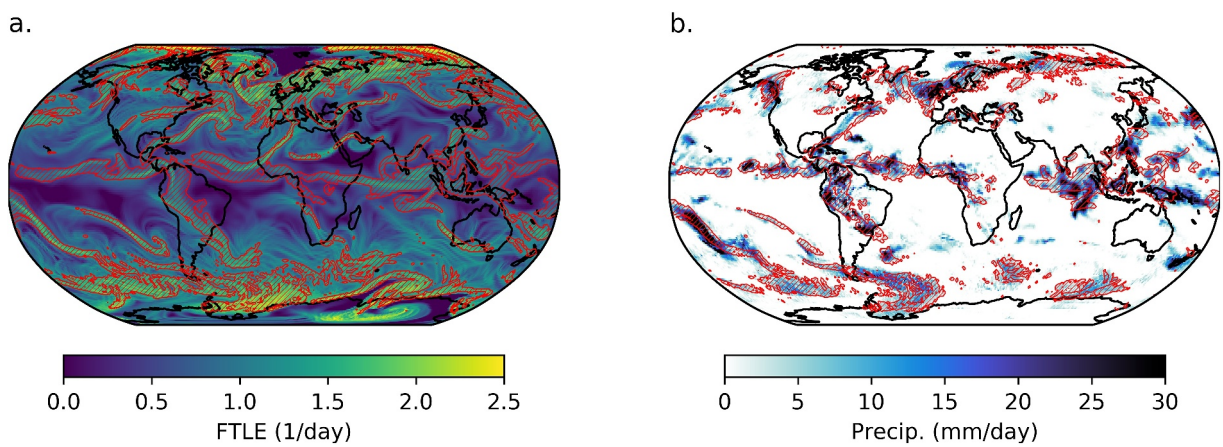

Figure 2. Example of the methodology to attribute precipitation to convergence zones (CZs) on 16 October 1996. (a) Finite-time Lyapunov exponent (FTLE) and CZ mask (red contours); the FTLE was computed using ERA5 (5th generation of the ECMWF atmospheric reanalysis). (b) GPCP-1DD (Global Precipitation Climatology Project) precipitation estimate on the same date; the red contours show where precipitation overlaps with the CZ mask.

4. Decomposition of Precipitation Error

We break down the precipitation errors associated with CZ and non-CZ events in terms of errors in frequency and intensity of precipitation. To this end, we employ the same bias decomposition approach employed by Catto et al. (2013, 2015) and Hawcroft et al. (2016) to assess frontal precipitation errors. Catto et al. (2015) provide a detailed explanation of this decomposition.

The precipitation error E_P can be written as a sum of the precipitation error during CZ events (E_{CZ}) and non-CZ events (E_{nCZ}):

$$E_P = E_{CZ} + E_{nCZ} \tag{2}$$

E_{CZ} and E_{nCZ} can be further decomposed in terms of frequency (ΔF_{CZ}, ΔF_{nCZ}) and intensity (ΔI_{CZ}, ΔI_{nCZ}) errors, where Δ denotes the difference between model and observation estimates. The first terms in the right-hand side (RHS) of Equations 3 and 4 are the errors in frequency of CZ and non-CZ events multiplied by the intensity of these events in observations ($I_{CZ,o}$ and $I_{nCZ,o}$, respectively). The second terms in the RHS of Equations 3 and 4 are the intensity errors of precipitation during CZ and non-CZ events multiplied by the average frequency of these events in observations ($F_{CZ,o}$ and $F_{nCZ,o}$). The last terms in the RHS are the mixed terms of errors in frequency and intensity of precipitation during these events.

$$E_{CZ} = \Delta F_{CZ} I_{CZ,\,o} + F_{CZ,\,o} \Delta I_{CZ} + \Delta F_{CZ} \Delta I_{CZ} \tag{3}$$

$$E_{nCZ} = \Delta F_{nCZ} I_{nCZ,o} + F_{nCZ,o} \Delta I_{nCZ} + \Delta F_{nCZ} \Delta I_{nCZ} \tag{4}$$

5. Models and Observations

In this study we employ historical simulations of six model instances from four model families of the Atmospheric Model Intercomparison Project (AMIP) submitted to CMIP6; we chose not to use the fully coupled simulations in order to focus on the role of atmospheric transport. This subset of simulations is chosen based on the availability of the 6-hourly outputs required to reproduce the methodology in Perez et al. (2021) and calculate the FTLE. The variables required are the horizontal wind components and water vapor concentration at a minimum of eight vertical levels. Simulations following the HighResMIP protocol (Haarsma et al., 2016), designed to answer questions related to systematic errors and tackle challenges of water availability (Eyring et al., 2016), present the required outputs; although a few simulations under other protocols present the required outputs, we restricted the analysis to HighResMIP. A summarized description of these models and an evaluation of their representation of the global hydrological is provided by Vannière et al. (2019).

As a best estimate, we employ ERA5 (Hersbach et al., 2020) to compute the FTLE, similarly to Perez et al. (2021, 2022). Because precipitation is a forecast variable in ERA5, we employ precipitation estimates from the GPCP 1° daily estimates (GPCP-1DD) (Huffman et al., 2001), from Climate Prediction Center morphing method (CMORPH) (Joyce et al., 2004) and from Integrated Multi-satellitE Retrievals for GPM (IMERG) (Huffman et al., 2020). The FTLE and precipitation from model and observational data sets are brought to a daily scale and interpolated to a common $1° \times 1°$ lat-lon grid. The time period we analyze in this study is 1996–2014; this range is limited by the first date available in GPCP-1DD and the final date in the CMIP6 present-climate simulations forced with observed sea-surface temperature. Table 1 lists the simulations and observational data sets and their characteristics.

6. Contribution of CZ Precipitation to Total Precipitation

6.1. Contribution in Observations

Figure 3 shows the mean GPCP-1DD precipitation (Figure 3a), the contributions of CZ (Figure 3b), and non-CZ (Figure 3c) events identified using ERA5 winds to the mean precipitation and the fraction of total precipitation associated with CZ events. In the regions where precipitation is higher (Figure 3a), such as the ITCZ, subtropical CZs and regions dominated by fronts, over 50% of the accumulated precipitation falls over CZs (Figure 3c). In dry regions, such as the subtropical highs and deserts, the contribution of CZs is typically below 10%. In a global average, approximately 53% of precipitation falls during CZ events when GPCP-1DD precipitation is considered.

Table 1
Coupled Model Intercomparison Project 6 Present-Climate Simulations and Observational Data Sets Employed in This Study

Data set	Members	Period	Coverage	Resolution (km)	Type
EC-Earth3P	3	1950–2014	Global	100	AMIP
EC-Earth3P-HR	2	1950–2014	Global	50	AMIP
ECMWF-IFS-HR	2	1950–2014	Global	25	AMIP
CNRM-CM6-1	1	1950–2014	Global	250	AMIP
CNRM-CM6-1-HR	1	1950–2014	Global	50	AMIP
HadGEM3-GC31-LM	1	1950–2014	Global	135	AMIP
ERA5	1	1950–Present	Global	30	Reanalysis
GPCP-1DD	1	1996–Present	Global	100	Satellite-related
CMORPH	1	2002–Present	60°S–60°N	30	Satellite-related
IMERG	1	2000–Present	60°S–60°N	10	Satellite-related

Note. The spatial resolution is presented as an approximation of the lat-lon grid spacing at the equator.

Between 60°S and 60°N, the estimated contribution of CZs to global precipitation is approximately 54% in GPCP-1DD, 51% in CMORPH, 59% in IMERG, and 67% in ERA5. Spatial maps showing the contribution of CZs to total precipitation using CMORPH, ERA5, and IMERG precipitation data can be found in Supporting Information S1.

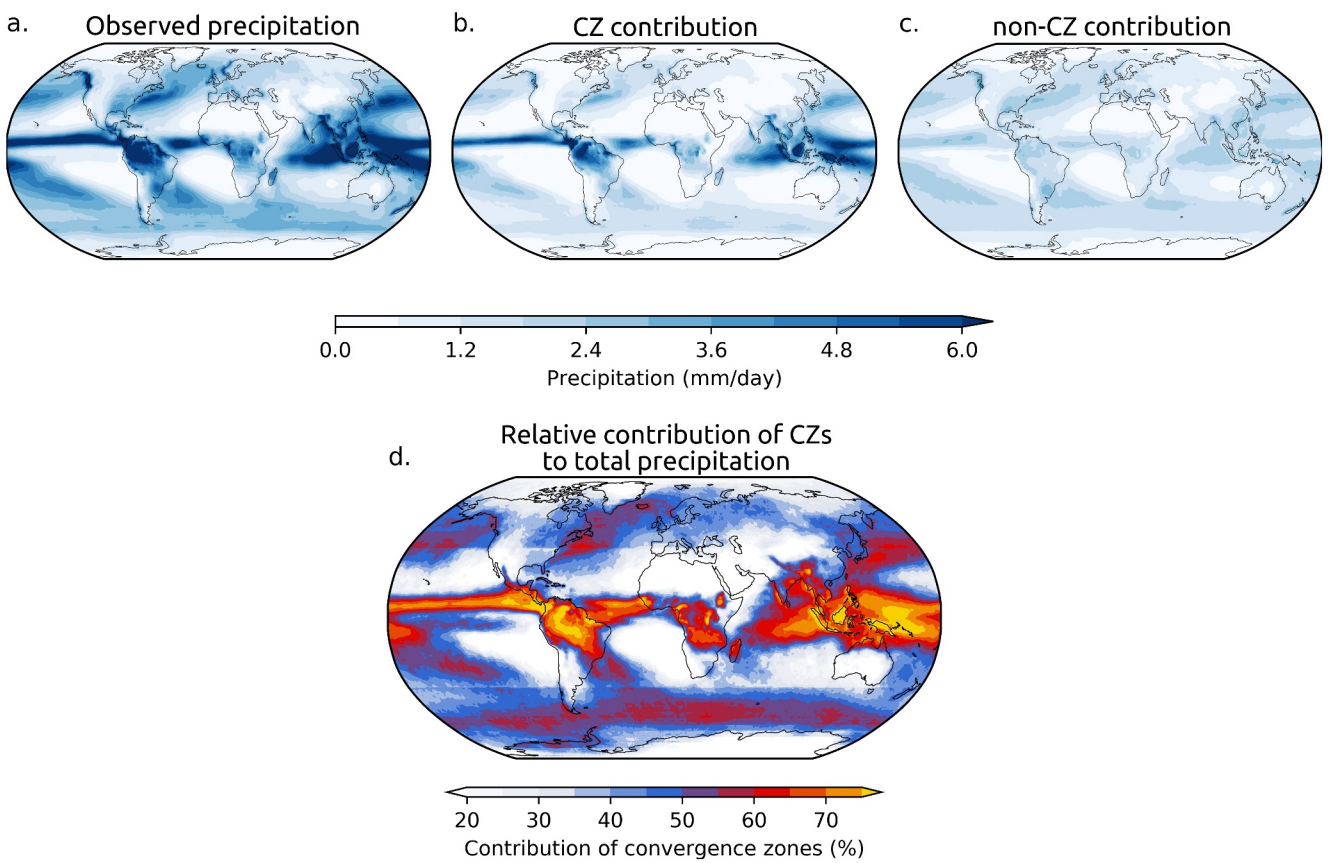

Figure 3. (a) Mean GPCP-1DD precipitation, (b) contribution of convergence zone (CZ), and (c) non-CZ events to the mean precipitation. (d) Fraction of the total precipitation allocated to CZs (i.e., the ratio between subplots "b" and "a").

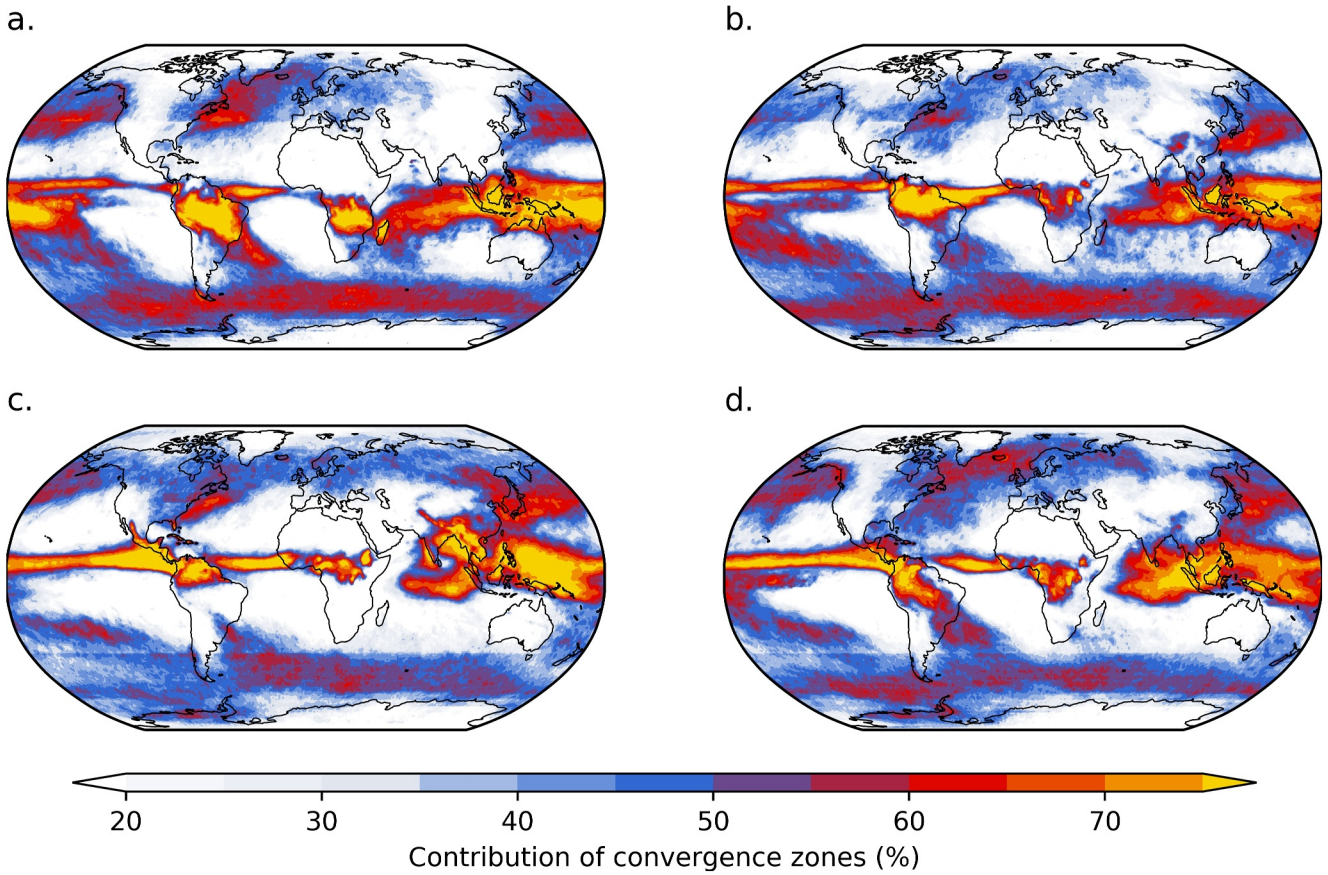

Figure 4. Fraction of total GPCP-1DD precipitation allocated to convergence zones identified using ERA5 winds in (a) DJF, (b) MAM, (c) JJA, and (d) SON.

We expect uncertainties in the estimated CZ contribution to originate from the observational limitations of precipitation products rather than from the FTLE. This is expected because (a) the FTLE is derived from large-scale reanalysis wind and (b) the formation of tracer filaments is robust to errors in the wind field (Methven & Hoskins, 1999). A first estimate of uncertainty can be achieved by comparing the CZ contribution in GPCP (54%), CMORPH (51%), and IMERG (59%): the difference between the highest and lowest estimates is 8%. A more robust assessment of uncertainty could be achieved by using other observational precipitation products.

Figure 4 shows the contribution of CZs to the total precipitation grouped by season (DJF, MAM, JJA, and SON) using GPCP-1DD precipitation data. In the equatorial region, contours above 70% reveal the seasonal migration of the ITCZ. In DJF, over 70% of precipitation in the monsoon regions in South America and South Africa falls during CZ events; these regions are known to be affected by the migrations of the ITCZ and the occurrence of the South Atlantic CZ (SACZ) and South Indian CZ. Still in DJF, we note that over 60% of precipitation in the South Pacific CZ (SPCZ) and the North Atlantic storm-track falls during CZ events. In MAM and JJA, we highlight the 60% contour close to Japan, marking the region of the Baiu front, a subtropical CZ with similar characteristics to the SACZ and the SPCZ (Kodama, 1992). In JJA, over 70% of precipitation falls during CZ events in parts of southeast Asia. Also noticeable in all seasons except MAM is the 60% contour along the East Coast of the United States of America; this contour roughly overlaps with the low-level atmospheric convergence generated by the Gulf stream (Kuwano-Yoshida et al., 2010).

6.2. Contribution in Climate Models

Figure 5 shows the apportionment of precipitation to CZ and non-CZ events in CMIP6 simulations compared with the observational estimates (i.e., CZs found with ERA5 winds and assigned precipitation from GPCP-1DD, CMORPH, and ERA5). When compared to GPCP-1DD and CMORPH estimates, all climate models allocate more precipitation to CZ events (Figure 5a) and less precipitation to non-CZ events (Figure 5b). This results in a

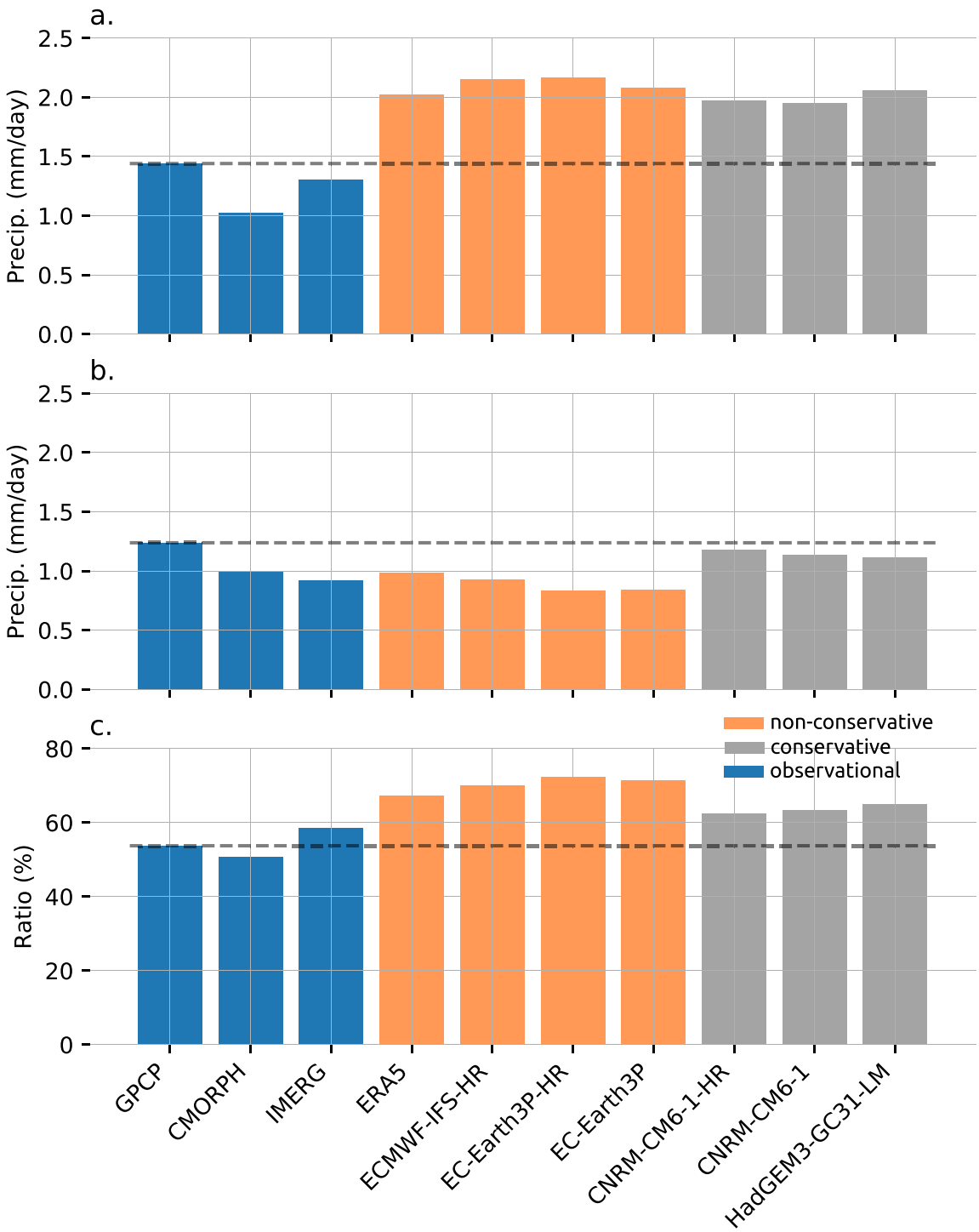

Figure 5. Contribution to the precipitation mean of: (a) convergence zone (CZ) events and (b) non-CZ events. (c) Relative contribution of CZ precipitation to the total precipitation. The horizontal dashed lines are marking GPCP-1DD estimate for comparison. The domain considered here is limited between 60°S and 60°N due to Climate Prediction Center morphing method's spatial coverage. Differences between simulations using the same model are negligible (three orders of magnitude smaller than the values presented), therefore, the ensemble mean is shown for the EC-Earth3P, EC-Earth3P-HR, and ECMWF-IFS-HR. Models with conservative and non-conservative moisture advection schemes are shown in gray and orange, respectively.

higher relative contribution of CZ precipitation than expected from observations (Figure 5c). We highlight that the precipitation apportionment to CZs in CNRM-CM6-1, CNRM-CM6-1-HR, and HadGEM3-GC31-LM is closer to the GPCP-1DD and CMORPH estimates than the other models. The apportionment using ERA5

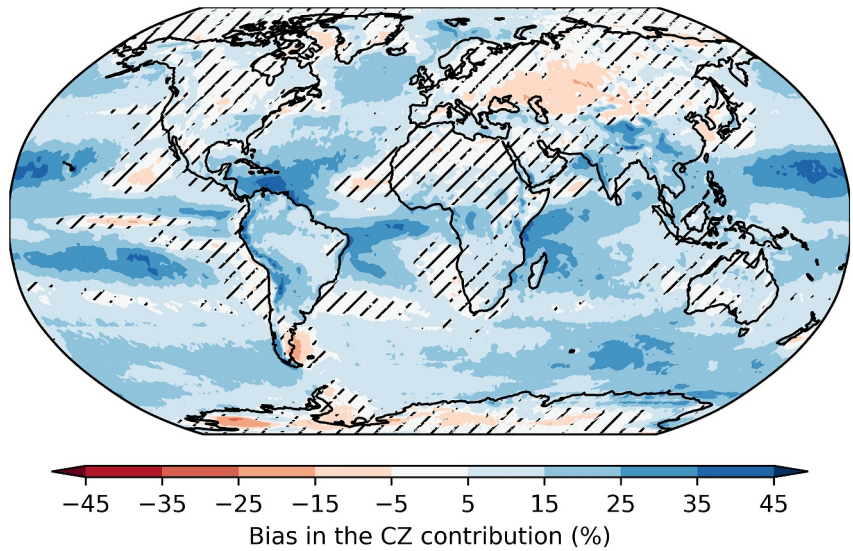

Figure 6. Percentual bias, averaged across models, of the contribution convergence zone (CZ) events to the precipitation mean. The bias of each climate model is obtained by comparing it with estimates using ERA5 CZs and GPCP-1DD precipitation. Hatched biases are not significant at the 1% level based on a Student's *t*-test.

precipitation is closer to the climate models than to GPCP-1DD and CMORPH, which is expected considering that precipitation is a forecast variable in reanalyses.

Figure 6 shows the percentual bias, averaged among models, of the contribution of CZs to precipitation when compared to the GPCP-1DD estimates. On average, climate models assign more precipitation to CZs especially in the tropics and some storm-track regions (e.g., North Atlantic and southern Indian). Around the Pacific ITCZ, we notice positive percentual biases higher than 25%; this is the region where the systematic double-ITCZ bias occurs in CMIP6 models (Tian & Dong, 2020). In the equatorial Atlantic, biases greater than 25% also coincide with displacement errors in the simulation of the Atlantic ITCZ (Richter & Tokinaga, 2020). Negative biases are found over the Eurasian continent, the equatorial eastern Pacific, and along the southern coast of Argentina. Positive biases along mountainous regions such as the Andes indicate an exaggerated model response to orography or unreliability of observational precipitation data sets in those regions. To further investigate the sources of precipitation biases, the next section presents the error decomposition in terms of frequency and intensity of CZ and non-CZ precipitation.

7. Decomposition of Frequency and Intensity Precipitation Biases

Figure 7 shows the average across models of the error terms on the RHS of Equations 3 and 4; the observational reference is obtained from CZs found using ERA5 winds and precipitation from GPCP-1DD. We first notice that the largest biases come from the frequency terms (ΔF): CZ precipitation shows predominantly positive biases (term $\Delta F_{\mathrm{CZ}} \times I_{\mathrm{CZ,o}}$) while non-CZ precipitation biases are predominantly negative (term $\Delta F_{\mathrm{nCZ}} \times I_{\mathrm{nCZ,o}}$). We highlight the signature of the double-ITCZ bias in the eastern equatorial Pacific in the frequency of CZ precipitation ($\Delta F_{\mathrm{CZ}} \times I_{\mathrm{CZ,o}}$); the frequency of non-CZ precipitation ($\Delta F_{\mathrm{nCZ}} \times I_{\mathrm{nCZ,o}}$) does not show the double-ITCZ signature, although, in many other tropical regions, its negative biases compensate the positive biases in the frequency of CZ precipitation.

The biases associated with intensity errors (ΔI) present both positive and negative values. There is a positive bias along the northeastern coast of South America that is particularly strong in the intensity of CZ precipitation ($\Delta I_{\mathrm{CZ}} \times F_{\mathrm{CZ,o}}$), indicating a displacement of the Atlantic ITCZ. One of the strongest errors in the intensity of non-CZ precipitation ($\Delta I_{\mathrm{nCZ}} \times F_{\mathrm{nCZ,o}}$) is in the region dominated by mesoscale convective complexes (MCCs) in southern South America (Durkee et al., 2009). MCCs are driven by the vertical shear between the low-level jet along the Andes and the subtropical jet (Mulholland et al., 2018); they are indeed not expected to be caused by CZs. The magnitudes of the biases in the mixed terms ($\Delta I_{\mathrm{CZ}} \times \Delta F_{\mathrm{CZ}}$ and $\Delta I_{\mathrm{nCZ}} \times \Delta F_{\mathrm{nCZ}}$) are much smaller than the other terms.

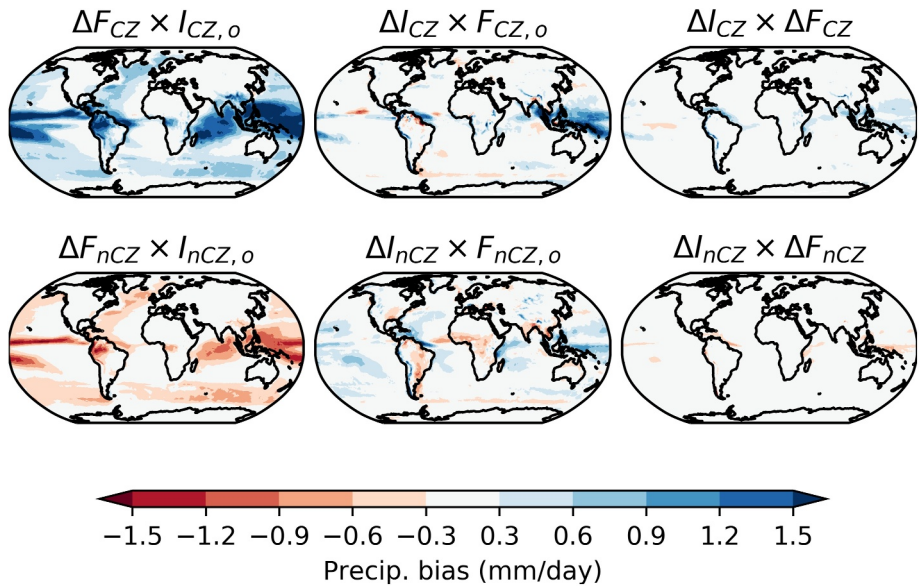

Figure 7. Decomposition of the precipitation biases in terms of frequency (ΔF) and intensity (ΔI) for convergence zone (CZ) and non-CZ events. Each term represents the average of the Coupled Model Intercomparison Project 6 simulations employed here. See Section 4 for details.

Figure 8 aggregates all the terms on the RHS of Equations 3 and 4 to compose the CZ and non-CZ precipitation errors (E_{CZ} and E_{nCZ}) in DJF and JJA. In both seasons, E_{CZ} is predominantly positive while E_{nCZ} is predominantly negative. In JJA we notice a strong negative bias in the Atlantic ITCZ sided by a positive bias along the northeastern coast of South America, indicating an error in the position of the ITCZ. In the DJF North Atlantic and the JJA South Indian ocean, storm-track regions present positive precipitation biases during CZ events and negative biases during non-CZ events. We also highlight the strong diagonal positive bias of CZ precipitation in the South Pacific in DJF, indicating that climate models exaggerate the SPCZ precipitation.

We can average the error terms spatially to see how they vary across simulations (Figure 9). We notice that, in all simulations, the error in CZ precipitation is dominated by positive frequency biases. In terms of non-CZ precipitation, all simulations present negative frequency biases. The mixed terms ($\Delta F \Delta I$) remain small for both CZ

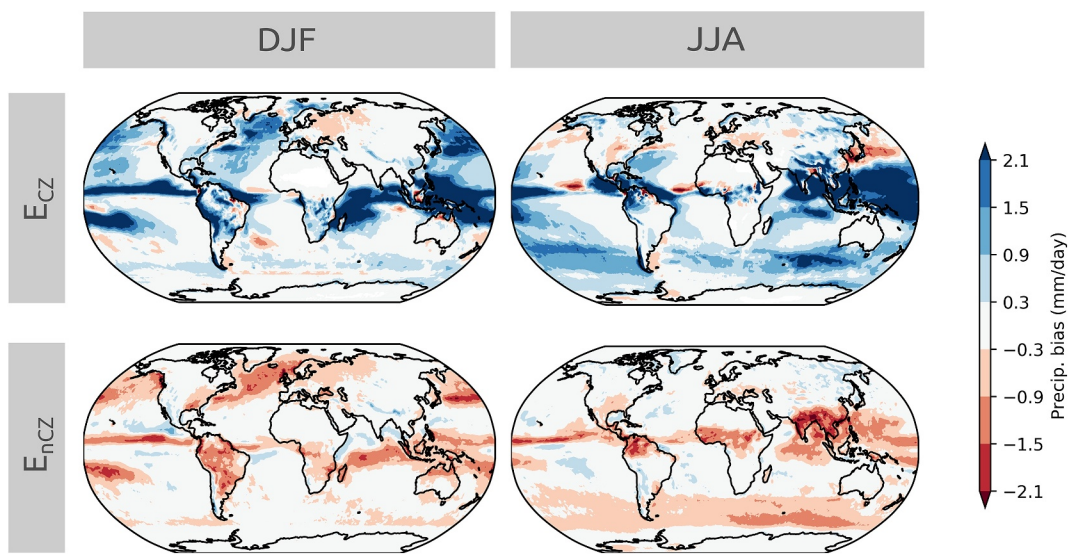

Figure 8. Precipitation errors associated with convergence zone (CZ) (E_{CZ}) and non-CZ events (E_{nCZ}) averaged across all simulations.

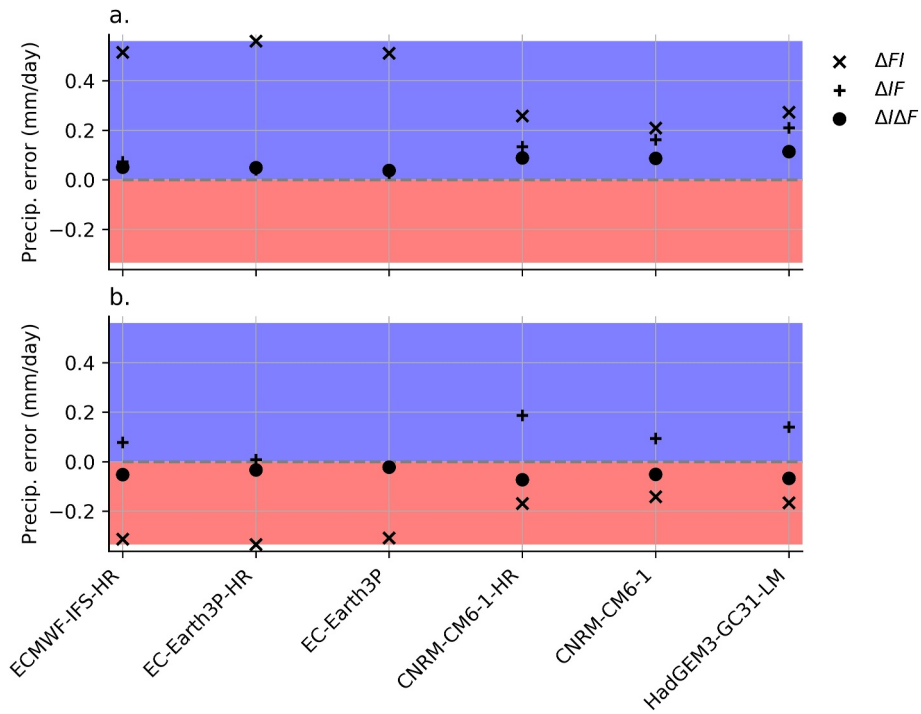

Figure 9. Spatial average of the model precipitation bias for (a) convergence zone (CZ) events and (b) non-CZ events.

and non-CZ precipitation. We highlight that CNRM-CM6-1, CNRM-CM6-1-HR, and HadGEM-GC31-LM present smaller biases in the frequency of CZ and non-CZ precipitation (although their intensity bias is higher); this helps explain the better representation of the apportionment of CZ precipitation in that model (see Figure 5). However, the smaller frequency bias of that model could be caused by cancellation of positive and negative biases in the spatial averaging. To verify if this is the case, Figure 10 shows the spatial average of the absolute value of the bias components. Indeed, the same three models mentioned above present smaller frequency errors, but the intensity errors are larger than in the other models.

8. Conclusion

In this study we quantify the contribution of CZs to precipitation by employing an objective diagnostic based on the degree of mixing of the synoptic-scale horizontal flow. We find that approximately 54% of global precipitation falls within CZ events. This quantification is enabled by the recent developments in Perez et al. (2021, 2022), who adapted a Lagrangian framework to identify atmospheric structures where the flow kinematics favors the accumulation of moisture. To the best of our knowledge, the only other similar global quantification of CZ precipitation is presented in Weller et al. (2017). There are two key distinctions between their methodology and the one employed here: (a) the convergence lines in Weller et al. (2017) are identified with an Eulerian diagnostic applied over a 6-hourly wind field, whilst here we employ a Lagrangian diagnostic calculated over 2-day trajectories to focus on synoptic-scale processes and (b) Weller et al. (2017) ascribe precipitation to convergence lines based on a fixed-distance mask of 2° on a lat-lon grid; in our case, the shape of our CZ mask is variable and based only on the FTLE value. Nonetheless, over oceanic regions our apportionment of precipitation to CZs and their apportionment to convergence lines is similar; over land, however, our CZ precipitation features are smoother. We expect this to be the case because the low-level flow over the ocean is typically steadier, leading to a better agreement between Lagrangian and Eulerian diagnostics.

When evaluating AMIP simulations submitted to CMIP6, we find that climate models overestimate the ratio of the total precipitation that falls during CZ events: observations suggest 54% (GPCP-1DD), 51% (CMORPH), and 59% (IMERG) while all climate models and ERA5 present a ratio above 60%; CNRM-CM6-1, CNRM-CM6-1-HR, and HadGEM3-GC31-LM present the ratio closest to the observations. Differently from the other models analyzed, these three climate models nearly close the water budget (Figure 9h in Vannière et al. (2019)); CNRM-

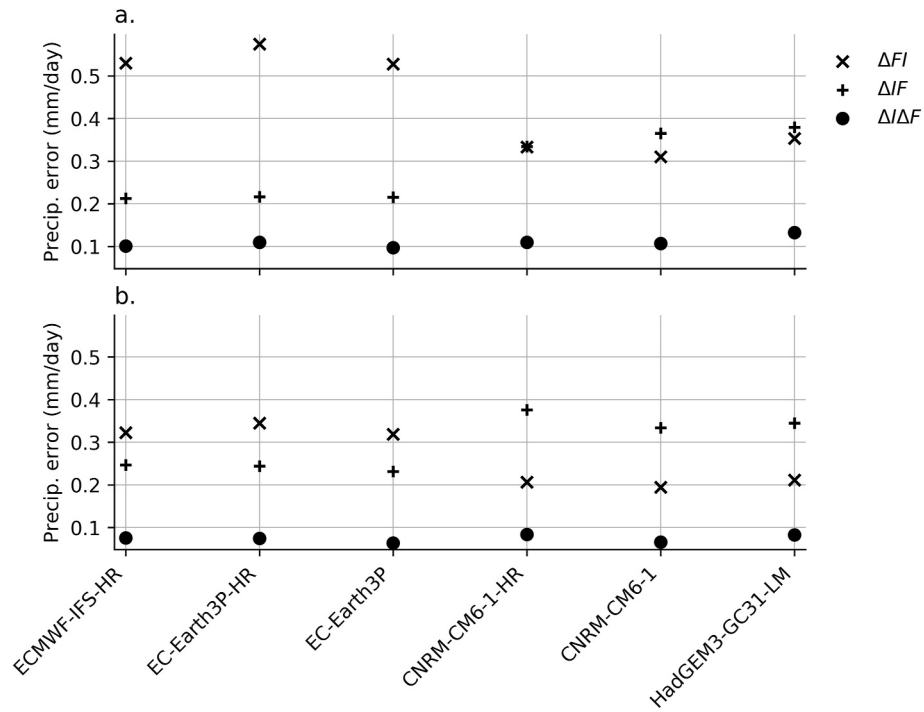

Figure 10. Spatial average of the absolute model precipitation bias for (a) convergence zone (CZ) events and (b) non-CZ events.

CM6 do so due to a mass conserving procedure applied at every time step to the semi-Lagrangian advection scheme (Voldoire et al., 2013). In, EC-Earth3P, a non-conserving model, for example, global precipitation exceeds evaporation by approx. 0.1 mm/day (derived from Figure 9h in Vannière et al. (2019)). This excess of precipitation due to non-conservative advection schemes could be amplified in regions of high mixing where horizontal gradients tend to be sharper; Dacre (2010) shows that the Met Office Unified Model overpredicts tracer concentration due to a non-conservative advection scheme, an issue that is more pronounced in regions where concentration gradients are sharper (i.e., airmass boundaries). Therefore, improved mass conservation in CNRM-CM6-1, CNRM-CM6-1-HR, and HadGEM3-GC31-LM may partly explain why these models allocate precipitation to high mixing events (CZs) in a proportion that is closer to observations than the other climate models.

We also show that the largest contribution to the precipitation error comes from a positive bias in the frequency of CZ precipitation. In other words, models trigger precipitation too frequently in situations of high mixing. This could be due to an exaggerated response of the convective parameterizations to the horizontal strain and accumulation of moisture in regions of high mixing. Indeed, some classes of climate models appear to underestimate the convective inhibition energy (Brockhaus et al., 2008), a problem that could potentially be alleviated in convection permitting simulations (Fosser et al., 2015). We also show that the signature of the double-ITCZ bias (Tian & Dong, 2020) is associated with errors in the frequency of CZ precipitation in the eastern equatorial Pacific.

The subset of simulations analyzed here is limited to the availability of 6-hourly winds and specific humidity outputs. Although submissions to CMIP6 under the HighResMIP protocol (Haarsma et al., 2016) as well as a few other AMIP6-type simulations present such variables, we found that many other simulations lack the required outputs. Considering the relevance of CZs to the global hydrological cycle, and to enable the reproduction of this diagnostic in a wider range of models, we recommend that future AMIP submissions output the required variables on at least eight vertical levels. Alternatively, 6-hourly outputs of the vertically integrated moisture flux and the total column water vapor can also be employed to compute mixing diagnostics and identify CZs (Perez et al., 2021).

Data Availability Statement

The ERA5 reanalysis data was obtained from the Copernicus data store (Hersbach et al., 2020). The CMIP6 simulations employed here were obtained from the WRCP platform (https://esgf-index1.ceda.ac.uk/projects/cmip6-ceda/) and submitted under the HighResMIP protocol (Haarsma et al., 2016). Code for identifying convergence zones is openly available at https://doi.org/10.5281/zenodo.4747229 (Perez, 2021).

Acknowledgments
This study was financed in part by the Coordenação de Aperfeiçoamento de Pessoal de Nível Superior–Brazil (CAPES)–Finance Code 88881.170642/2018-01, by the University of Reading, U. K and by MeteoIA, Brazil.

References

Brockhaus, P., Luthi, D., & Schar, C. (2008). Aspects of the diurnal cycle in a regional climate model. *Meteorologische Zeitschrift*, *17*(4), 433–444. https://doi.org/10.1127/0941-2948/2008/0316

Carvalho, L. M., Jones, C., & Liebmann, B. (2004). The South Atlantic convergence zone: Intensity, form, persistence, and relationships with intraseasonal to interannual activity and extreme rainfall. *Journal of Climate*, *17*(1), 88–108. https://doi.org/10.1175/1520-0442(2004)017<0088:tsaczi>2.0.co;2

Catto, J., Jakob, C., & Nicholls, N. (2013). A global evaluation of fronts and precipitation in the access model. *Australian Meteorological and Oceanographic Journal*, *63*(1), 191–203. https://doi.org/10.22499/2.6301.012

Catto, J., Jakob, C., & Nicholls, N. (2015). Can the cmip5 models represent winter frontal precipitation? *Geophysical Research Letters*, *42*(20), 8596–8604. https://doi.org/10.1002/2015gl066015

Chen, D., Dai, A., & Hall, A. (2021). The convective-to-total precipitation ratio and the "drizzling" bias in climate models. *Journal of Geophysical Research: Atmospheres*, *126*(16), e2020JD034198. https://doi.org/10.1029/2020jd034198

Cohen, R. A., & Kreitzberg, C. W. (1997). Airstream boundaries in numerical weather simulations. *Monthly Weather Review*, *125*(1), 168–183. https://doi.org/10.1175/1520-0493(1997)125<0168:abinws>2.0.co;2

Dacre, H. (2010). Evaluating the ability of a numerical weather prediction model to forecast tracer concentrations during ETEX 2. *Atmospheric Environment*, *44*(3), 294–303. https://doi.org/10.1016/j.atmosenv.2009.10.039

Durkee, J. D., Mote, T. L., & Shepherd, J. M. (2009). The contribution of mesoscale convective complexes to rainfall across subtropical South America. *Journal of Climate*, *22*(17), 4590–4605. https://doi.org/10.1175/2009jcli2858.1

Eyring, V., Bony, S., Meehl, G. A., Senior, C. A., Stevens, B., Stouffer, R. J., & Taylor, K. E. (2016). Overview of the coupled model intercomparison project phase 6 (CMIP6) experimental design and organization. *Geoscientific Model Development*, *9*(5), 1937–1958. https://doi.org/10.5194/gmd-9-1937-2016

Fosser, G., Khodayar, S., & Berg, P. (2015). Benefit of convection permitting climate model simulations in the representation of convective precipitation. *Climate Dynamics*, *44*(1), 45–60. https://doi.org/10.1007/s00382-014-2242-1

Franco-Diaz, A., Klingaman, N. P., Vidale, P. L., Guo, L., & Demory, M.-E. (2019). The contribution of tropical cyclones to the atmospheric branch of middle America's hydrological cycle using observed and reanalysis tracks. *Climate Dynamics*, *53*(9), 6145–6158. https://doi.org/10.1007/s00382-019-04920-z

Garaboa-Paz, D., Eiras-Barca, J., Huhn, F., & Pérez-Muñuzuri, V. (2015). Lagrangian coherent structures along atmospheric rivers. *Chaos: An Interdisciplinary Journal of Nonlinear Science*, *25*(6), 063105. https://doi.org/10.1063/1.4919768

Garaboa-Paz, D., Eiras-Barca, J., & Pérez-Muñuzuri, V. (2017). Climatology of Lyapunov exponents: The link between atmospheric rivers and large-scale mixing variability. *Earth System Dynamics*, *8*(3), 865–873. https://doi.org/10.5194/esd-8-865-2017

Guo, L., Klingaman, N. P., Vidale, P. L., Turner, A. G., Demory, M.-E., & Cobb, A. (2017). Contribution of tropical cyclones to atmospheric moisture transport and rainfall over East Asia. *Journal of Climate*, *30*(10), 3853–3865. https://doi.org/10.1175/jcli-d-16-0308.1

Haarsma, R. J., Roberts, M. J., Vidale, P. L., Senior, C. A., Bellucci, A., Bao, Q., et al. (2016). High resolution model intercomparison project (HIGHRESMIP v1. 0) for CMIP6 [Dataset]. *Geoscientific Model Development*, *9*(11), 4185–4208. https://doi.org/10.5194/gmd-9-4185-2016

Hawcroft, M. K., Shaffrey, L. C., Hodges, K. I., & Dacre, H. F. (2016). Can climate models represent the precipitation associated with extratropical cyclones? *Climate Dynamics*, *47*(3), 679–695. https://doi.org/10.1007/s00382-015-2863-z

Hersbach, H., Bell, B., Berrisford, P., Hirahara, S., Horányi, A., Muñoz-Sabater, J., et al. (2020). The ERA5 global reanalysis. *Quarterly Journal of the Royal Meteorological Society*, *146*(730), 1999–2049. https://doi.org/10.1002/qj.3803

Huffman, G. J., Adler, R. F., Morrissey, M. M., Bolvin, D. T., Curtis, S., Joyce, R., et al. (2001). Global precipitation at one-degree daily resolution from multisatellite observations. *Journal of Hydrometeorology*, *2*(1), 36–50. https://doi.org/10.1175/1525-7541(2001)002<0036:gpaodd>2.0.co;2

Huffman, G. J., Bolvin, D. T., Braithwaite, D., Hsu, K.-L., Joyce, R. J., Kidd, C., et al. (2020). Integrated multi-satellite retrievals for the global precipitation measurement (GPM) mission (IMERG). *Satellite Precipitation Measurement*, *1*, 343–353. https://doi.org/10.1007/978-3-030-24568-9_19

Joyce, R. J., Janowiak, J. E., Arkin, P. A., & Xie, P. (2004). CMORPH: A method that produces global precipitation estimates from passive microwave and infrared data at high spatial and temporal resolution. *Journal of Hydrometeorology*, *5*(3), 487–503. https://doi.org/10.1175/1525-7541(2004)005<0487:camtpg>2.0.co;2

Kodama, Y. (1992). Large-scale common features of subtropical precipitation zones (the Baiu frontal zone, the SPCZ, and the SACZ) part i: Characteristics of subtropical frontal zones. *Journal of the Meteorological Society of Japan. Ser. II*, *70*(4), 813–836. https://doi.org/10.2151/jmsj1965.70.4_813

Kuwano-Yoshida, A., Minobe, S., & Xie, S.-P. (2010). Precipitation response to the gulf stream in an atmospheric GCM. *Journal of Climate*, *23*(13), 3676–3698. https://doi.org/10.1175/2010jcli3261.1

Läderach, A., & Sodemann, H. (2016). A revised picture of the atmospheric moisture residence time. *Geophysical Research Letters*, *43*(2), 924–933. https://doi.org/10.1002/2015gl067449

Leung, L. R., Boos, W. R., Catto, J. L., A. DeMott, C., Martin, G. M., Neelin, J. D., et al. (2022). Exploratory precipitation metrics: Spatiotemporal characteristics, process-oriented, and phenomena-based. *Journal of Climate*, *35*(12), 3659–3686. https://doi.org/10.1175/jcli-d-21-0590.1

Li, Y., Yan, D., Peng, H., & Xiao, S. (2021). Evaluation of precipitation in CMIP6 over the Yangtze River Basin. *Atmospheric Research*, *253*, 105406. https://doi.org/10.1016/j.atmosres.2020.105406

Methven, J., & Hoskins, B. (1999). The advection of high-resolution tracers by low-resolution winds. *Journal of the Atmospheric Sciences*, *56*(18), 3262–3285. https://doi.org/10.1175/1520-0469(1999)056<3262:taohrt>2.0.co;2

Mulholland, J. P., Nesbitt, S. W., Trapp, R. J., Rasmussen, K. L., & Salio, P. V. (2018). Convective storm life cycle and environments near the Sierras de Córdoba, Argentina. *Monthly Weather Review*, *146*(8), 2541–2557. https://doi.org/10.1175/mwr-d-18-0081.1

Ottino, J. M. (1989). *The kinematics of mixing: Stretching, chaos, and transport* (Vol. 3). Cambridge university press.
Perez, G. M. P. (2021). Lagrangian coherence (v1.0.1) [Software]. https://doi.org/10.5281/zenodo.4747229
Perez, G. M. P., Vidale, P. L., Dacre, H., & García-Franco, J. L. (2022). Using a synoptic-scale mixing diagnostic to explain global precipitation variability from weekly to interannual time scales. *Journal of Climate*, *35*(24), 8225–8243. https://doi.org/10.1175/jcli-d-22-0110.1
Perez, G. M. P., Vidale, P. L., Klingaman, N. P., & Martin, T. (2021). Atmospheric convergence zones stemming from large-scale mixing. *Weather and Climate Dynamics*, *2*(2), 475–488. https://doi.org/10.5194/wcd-2-475-2021
Pierrehumbert, R. (1991). Large-scale horizontal mixing in planetary atmospheres. *Physics of Fluids A: Fluid Dynamics*, *3*(5), 1250–1260. https://doi.org/10.1063/1.858053
Richter, I., & Tokinaga, H. (2020). An overview of the performance of CMIP6 models in the tropical Atlantic: Mean state, variability, and remote impacts. *Climate Dynamics*, *55*(9), 2579–2601. https://doi.org/10.1007/s00382-020-05409-w
Shepherd, T. G., Koshyk, J. N., & Ngan, K. (2000). On the nature of large-scale mixing in the stratosphere and mesosphere. *Journal of Geophysical Research*, *105*(D10), 12433–12446. https://doi.org/10.1029/2000jd900133
Tian, B., & Dong, X. (2020). The double-ITCZ bias in CMIP3, CMIP5, and CMIP6 models based on annual mean precipitation. *Geophysical Research Letters*, *47*(8), e2020GL087232. https://doi.org/10.1029/2020gl087232
Van Der Wiel, K., Matthews, A. J., Joshi, M. M., & Stevens, D. P. (2016). The influence of diabatic heating in the South Pacific Convergence Zone on Rossby wave propagation and the mean flow. *Quarterly Journal of the Royal Meteorological Society*, *142*(695), 901–910. https://doi.org/10.1002/qj.2692
Vannière, B., Demory, M.-E., Vidale, P. L., Schiemann, R., Roberts, M. J., Roberts, C. D., et al. (2019). Multi-model evaluation of the sensitivity of the global energy budget and hydrological cycle to resolution. *Climate Dynamics*, *52*(11), 6817–6846. https://doi.org/10.1007/s00382-018-4547-y
Voldoire, A., Sanchez-Gomez, E., Salas y Mélia, D., Decharme, B., Cassou, C., Sénési, S., et al. (2013). The CNRM-CM5. 1 global climate model: Description and basic evaluation. *Climate Dynamics*, *40*(9), 2091–2121. https://doi.org/10.1007/s00382-011-1259-y
Welander, P. (1955). Studies on the general development of motion in a two-dimensional, ideal fluid. *Tellus*, *7*(2), 141–156. https://doi.org/10.1111/j.2153-3490.1955.tb01147.x
Weller, E., Shelton, K., Reeder, M. J., & Jakob, C. (2017). Precipitation associated with convergence lines. *Journal of Climate*, *30*(9), 3169–3183. https://doi.org/10.1175/jcli-d-16-0535.1
Zhou, W., Leung, L. R., & Lu, J. (2022). Linking large-scale double-ITCZ bias to local-scale drizzling bias in climate models. *Journal of Climate*, *35*(24), 7965–7979. https://doi.org/10.1175/jcli-d-22-0336.1